Pair dispersion over an inertial range spanning many decades

Frank W. Elliott, Jr. and Andrew J. Majda
Courant Institute of Mathematical Sciences, New York University, New York, New York 10012-1185

(Received 15 August 1995; accepted 8 December 1995)

New numerical results on scalar pair dispersion through an inertial range spanning many decades are presented here. These results are achieved through a new Monte Carlo algorithm for synthetic turbulent velocity fields, which has been developed and validated recently by the authors [J. Comput. Phys. **117**, 146 (1995)]; this algorithm is capable of accurate simulation of a Gaussian incompressible random field with the Kolmogoroff spectrum over 12–15 decades of scaling behavior with low variance. The numerical results for pair dispersion reported here are within the context of random velocity fields satisfying Taylor's hypothesis for two-dimensional incompressible flow fields. For the Kolmogoroff spectrum, Richardson's t^3 scaling law is confirmed over a range of pair separation distances spanning eight decades with a Richardson constant with the value 0.031 ± 0.004 over nearly eight decades of pair separation, provided that the longitudinal component of the velocity structure tensor is normalized to unity. Remarkably, in appropriate units this constant agrees with the one calculated by Tatarski's experiment from 1960 within the stated error bars. Other effects on pair dispersion of varying the energy spectrum of the velocity field and the degree of isotropy, as well as the importance of rare events in pair separation statistics, are also developed here within the context of synthetic turbulence satisfying Taylor's hypothesis. © *1996 American Institute of Physics.* [S1070-6631(96)00504-7]

I. INTRODUCTION

Pair dispersion is the simplest and most important statistic, which is a manifestation of the inverse cascade of a passive scalar through a range of turbulent velocity scales. After Richardson's pioneering work with his famous t^3 law, a large effort has focused on predicting and confirming this law and its associated fundamental preconstant through actual experiments,[2,3] turbulence closure theories,[4,7] and numerical simulation.[8–10]

Here we present the first numerical experiments, which confirm Richardson's t^3 law over many decades of pair separation and also give a value of the preconstant for pair dispersion that settles down to a constant within small errors over many decades. In both instances our results are valid over nearly eight decades of pair separation. To achieve these results for pair dispersion, we utilize a novel Monte Carlo method for generating synthetic, incompressible, Gaussian random velocity fields devised recently by the authors; this new method is capable of generating fractal velocity fields with the Kolmogoroff spectrum with low variance and high accuracy for both the prefactor and scaling exponent for the velocity structure function over 12 decades.[11] Furthermore, the basic algorithm has already been validated for applications in turbulent diffusion[11] including pair dispersion on an exactly solvable model involving random shear layers.[13,14] In contrast, the results on pair dispersion via synthetic turbulence that are reported in Refs. 8 and 10 involve numerical methods, where the velocity structure function has the Kolmogoroff scaling for roughly one decade (for example, see Fig. 5 of Ref. 10) with a similar range for typical direct simulations involving fluid equations.[9]

Here, we consider pair separation statistics for a passive scalar transported by an incompressible velocity field in two space dimensions under Taylor's hypothesis. Thus, the basic passive scalar transport problem has the form

$$\frac{\partial T}{\partial t} + \mathbf{v}(\mathbf{x} + \bar{w}t) \cdot \nabla T = 0, \tag{1}$$

where $\bar{w} \neq 0$ is the large-scale sweeping velocity and $\mathrm{div}(\mathbf{v}) = 0$. The random velocity fields in (1) are the simplest ones compatible with the statistical component of the velocity field satisfying Taylor's hypothesis. We remark that the energy-power spectrum $E(\mathbf{k},\omega)$ for the velocity field, $\mathbf{v}$, satisfies $E(\mathbf{k},\omega) = \delta(\omega - \mathbf{k}\bar{w})E_0(\mathbf{k})$, where $E_0(\mathbf{k})$ is the spatial energy spectrum of $\mathbf{v}(\mathbf{x})$, $\bar{w}$ is the large-scale sweeping direction, and δ is the Dirac-delta function. For this random velocity field, the temporal correlations at a fixed point in time are a simple scaling through the mean sweep $\bar{w}$ of the spatial correlations in the direction $\bar{w}$, and this is the essential feature of Taylor's hypothesis. However, we also note that the velocity field in (1) has mean zero so the explicit effect of the constant mean field has been removed. Thus, the statistical piece of the flow has the statistics of Taylor's hypothesis without an explicit mean flow advection.

We assume that the incompressible velocity field, $\mathbf{v}(\mathbf{x})$, is a Gaussian fractal field with mean zero, $\langle \mathbf{v} \rangle = 0$, and scaling behavior for the velocity differences given by

$$\langle |\mathbf{v}(\mathbf{x} + \mathbf{x}') - \mathbf{v}(\mathbf{x}')|^2 \rangle = C_{\mathrm{H}} |\mathbf{x}|^{2\mathrm{H}}, \tag{2}$$

for $l_d < |\mathbf{x}| \leqslant 1$ and for $0 < H < 1$ with H the Hurst exponent and l_d roughly the dissipation length scale. The familiar Kolmogoroff spectrum corresponds to the value $H = \frac{1}{3}$, with $C_{\mathrm{H}} = C\bar{\epsilon}^{2/3}$, $\bar{\epsilon}$ is the dissipation rate, and C, the Kolmogoroff constant for the velocity difference. In our main simulation presented in Sec. III for pair dispersion in a velocity field with Kolmogoroff scaling, we have $l_d = 10^{-15}$ with reliable accuracy over this entire intertial range generated by our synthetic turbulence algorithm.[12]

 1070-6631/96/8(4)/1052/9/$10.00

We study the statistics of pair separation for the passive scalar problem in (1). Thus, we take two particles $\mathbf{X}_j$ for $j=1,2$ with a fixed initial separation distance s, so that

$$|\mathbf{X}_1^t-\mathbf{X}_2^t|=s, \tag{3}$$

and follow the pair separation,

$$\mathbf{X}_1^t-\mathbf{X}_2^t, \quad \text{for } t>0, \tag{4}$$

where each particle is advected by the random velocity field, $\mathbf{v}(\mathbf{x}+\bar{w}t)$, from (1). The pair separation, $\mathbf{X}_1^t-\mathbf{X}_2^t$, is a random variable depending on the velocity statistics and the pair dispersion, $\sigma^2(t,s)$, is the second moment of this random variable,

$$\langle|\mathbf{X}_1^t-\mathbf{X}_2^t|^2\rangle=\sigma^2(t,s), \tag{5}$$

where $\langle\cdot\rangle$ denotes ensemble averaging over the random velocity field. Next, we briefly summarize the remainder of this paper. Our choice of nondimensionalization and the numerical method for (1) are discussed in Sec. II. The main new feature of the Monte Carlo method beyond the parts already developed and validated in Refs. 11 and 12 is an adaptive time step strategy for pair separation that we validate for velocity fields with the Kolmogoroff spectrum in Sec. II. It is worth emphasizing here that in Sec. II we nondimensionalize the longitudinal velocity structure constant to have the value 1 in all of our simulations. This facilitates simple comparison between the results presented here and earlier work for both two- and three-dimensional flows. This discussion occurs in Sec. VI. The main results of this paper are presented in Sec. III, where, with the Kolmogoroff spectrum, we verify Richardson's t^3 law with an accurate constant for pair dispersion over nearly eight decades of pair separation,

$$\sigma^2(t)=\beta t^3 \quad \text{and} \quad \beta=0.031\pm0.004, \tag{6}$$

with the nondimensionalization mentioned earlier. In Sec. III we also study the occurrence of rare events in pair separation statistics. We study the effects of an anisotropic Kolmogoroff spectrum on pair dispersion statistics in Sec. IV. In Sec. V we present numerical evidence, which confirms the universal scaling law for pair dispersion,[6,9]

$$\sigma^2(t)=\beta_{\mathrm{H}}t^{2/(1-H)}, \quad \text{for } \sigma(t)\gg s, \tag{7}$$

for $0<H<\frac{1}{2}$ as the spectrum of the velocity field from (1) is varied. Finally, in Sec. VI we compare and contrast our results with other work on pair dispersion and discuss some future directions under current investigation by the authors.

II. PRELIMINARIES

A. Nondimensionalization

For the velocity field defined in (2) and given any length scale, l, there are two natural time scales associated with the scalar problem from (1), the sweep time, $\tau_s(l)$, and the eddy turnover time, $\tau_e(l)$. The sweep time, $\tau_s(l)$, is given by

$$\tau_s(l)=\frac{l}{|\bar{w}|}. \tag{8}$$

We utilize a normalization of the eddy turnover time that is natural for studying pair separation statistics.

If $l(t)=|\mathbf{X}_1^t-\mathbf{X}_2^t|$ is the separation distance in a given realization, then from (1) we derive that

$$\frac{d}{dt}\frac{1}{2}l^2(t)=[\mathbf{v}(\mathbf{X}_1^t+\bar{w}t)-\mathbf{v}(\mathbf{X}_2^t+\bar{w}t)]\cdot(\mathbf{X}_1^t-\mathbf{X}_2^t). \tag{9}$$

From the formula in (9), it follows that pair separation statistics are primarily sensitive to longitudinal displacements of the velocity field. For an isotropic, incompressible Gaussian field with the structure function in Eq. (2) in d space dimensions, the longitudinal component of the velocity structure tensor is given by

$$\left\langle\left([\mathbf{v}(\mathbf{x}+\mathbf{x}')-\mathbf{v}(\mathbf{x}')]\cdot\frac{\mathbf{x}}{|\mathbf{x}|}\right)^2\right\rangle=\tilde{C}_{\mathrm{H}}^2|\mathbf{x}|^{2\mathrm{H}}, \tag{10}$$

while the full magnitude of the velocity difference is

$$\langle|\mathbf{v}(\mathbf{x}+\mathbf{x}')-\mathbf{v}(\mathbf{x}')|^2\rangle=(2H+d)\tilde{C}_{\mathrm{H}}^2|\mathbf{x}|^{2\mathrm{H}}, \tag{11}$$

i.e. $C_{\mathrm{H}}=(2H+d)\tilde{C}_{\mathrm{H}}^2$ in Eq. (2).[3,12] With all of the above information from (9) and (10), the natural definition of eddy turnover time, $\tau_e(l)$, in studying pair separation statistics, is to utilize the longitudinal velocity displacements and define

$$\tau_e(l)=\tilde{C}_{\mathrm{H}}^{-1}l^{1-H}. \tag{12}$$

With the definitions for sweep time and eddy turnover time in (8) and (12), we define the unit of length through the scale l, where $\tau_e(l)=\tau_s(l)$, i.e. where the sweep time equals the eddy turnover time, and we define the unit of time through $\tau_e(l)=\tau_s(l)$. With this choice of nondimensionalization, we have the scalar transport problem in (1) with the normalizations

$$\begin{aligned}&\tilde{C}_{\mathrm{H}}=1, \quad |\bar{w}|=1,\\ &\tau_e(l)=l^{\mathrm{H}-1}, \quad \tau_s(l)=l,\end{aligned} \tag{13}$$

which we assume in presenting our results throughout this paper. We remark that the sweep time and eddy turnover time satisfy

$$\tau_s(l)\ll\tau_e(l), \quad \text{for } l\ll 1, \tag{14}$$

so that we have arranged in our numerical experiments for the standard conditions where Taylor's hypothesis is usually assumed in interpreting experimental data.[3]

B. The numerical method

An algorithm for evaluating pair separation statistics requires two main features: first, a Monte Carlo method for simulating an isotropic incompressible Gaussian random field satisfying the scaling relations in (2) and (10) over as many decades of spatial scaling as possible, and second, a discrete time stepping procedure. We use the Monte Carlo algorithm devised in Ref. 12 for simulating an isotropic incompressible Gaussian field; the lengthy validation studies in Ref. 12 verify that this algorithm is capable of satisfying the scaling relations in (2) and (10) over 12–15 decades with low statistical variance involving only 100 to 1000 realizations, yielding the exponent H exact to four significant figures and the preconstant $\tilde{C}_{\mathrm{H}}$ exact to within 5% over the entire range of scales. This algorithm[12] combines random plane waves[15] with suitable explicit one-dimensional wave-

lets with high moment cancellation;[11] a leisurely introduction to the basic design of the algorithm in one space dimension can be found in Ref. 16. The high resolution capabilities of this Monte Carlo algorithm allow us to pick initial particle separation distances as small as $s=10^{-14}$ in the numerical experiments described below. In Ref. 12 we have verified that a field with 16 plane waves (over 32 shearing directions) achieved a high degree of isotropy, and this value is used in all the isotropic simulations reported below in Secs. III and IV. We also guarantee that the mean flow $\bar{w}$ does not align exactly with any of these directions.

The smallest time scale in the problem is the sweep time at the dissipation scale $\tau_s(l_d)$, and the most straightforward time step criterion would involve a fixed small multiple of $\tau_s(l_d)$. However, in attempting to simulate pair separation statistics over a large number of decades of separation, such a straightforward strategy is hopelessly expensive and impractical. Instead, with the formula in (9) as motivation, given the locations, $\mathbf{X}_1^t$ and $\mathbf{X}_2^t$, of the particle pair in a given realization, we adopt a variable time step based on the rate of separation of the two particles; thus we set

$$\Delta t=\alpha l(t)\left|\frac{d}{dt}\, l(t)\right|^{-1}, \tag{15}$$

for $\alpha<1$ a fixed constant and utilize Euler's method with this time step size in our integration of pair separation statistics, where we use the formula in (9) to evaluate $dl(t)/dt$ for each realization. Since formula (8) implies that the denominator in formula (15) depends on the difference of two nearly equal numbers, it is necessary to do the computation in 64-bit arithmetic to avoid division by 0. We note that in the simulations reported below, in each realization we begin with only one pair of particles at a fixed separation distance, so the above time stepping procedure is well defined.

Why do we use the simple, low-order Euler's method for time integration rather than higher-order time stepping? There are two reasons. First, we are computing with nowhere differentiable velocity fields, and it is well known that higher-order time stepping only improves the accuracy for smooth velocity fields. Second, the computational overhead in the variable time-step strategy with a higher-order method is significant compared to the first-order method. David Horntrop (private communication)[19] has compared the first-order Euler method with higher-order time-stepping procedures on the exactly solvable model from Refs. 13 and 14 with nonsmooth velocity fields and has verified the above behavior for higher-order methods. Next, we validate the time stepping criterion in (15) and demonstrate its convergence for $\alpha\ll 1$.

C. Validation study of the variable time-step strategy

To validate the time-stepping procedure, we ran the basic algorithm with the Kolmogoroff spectrum, $H=\frac{1}{3}$, and varied the time step strategy through the values $\alpha=\frac{1}{2}$, $\frac{1}{4}$, $\frac{1}{8}$, and $\frac{1}{16}$. We used an initial pair separation distance, $s=10^{-12}$ and computed the RMS pair dispersion $\sigma(t)$, defined earlier in (6), by averaging over 1024 realizations utilizing the adaptive time-step strategy described above for each realization.

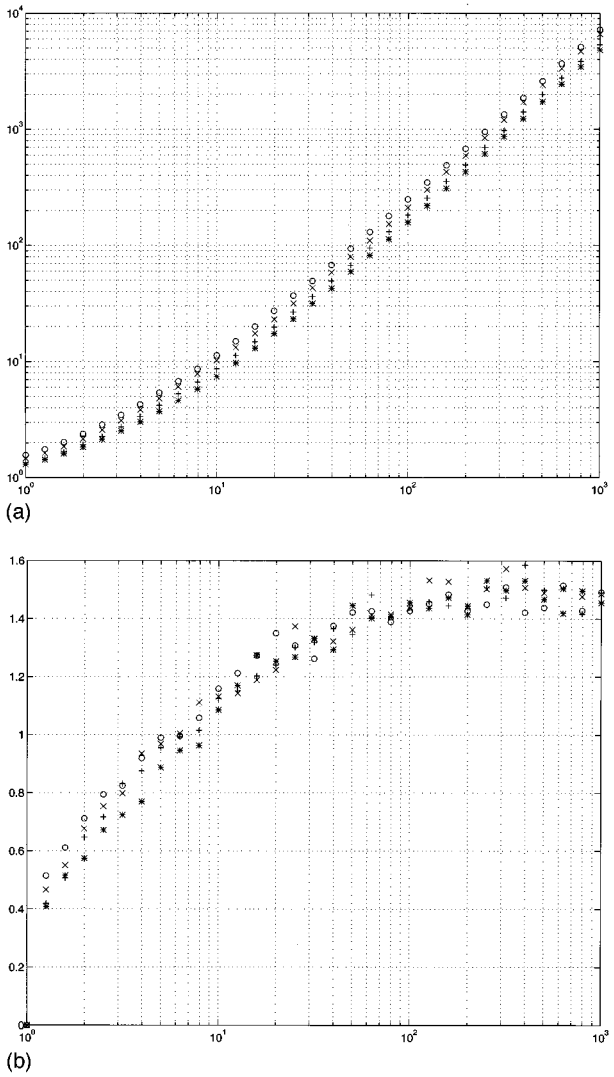

FIG. 1. Plots of (a) RMS dispersion versus time; (b) the logarithmic derivative of RMS dispersion versus time with Hurst exponent $H=\frac{1}{3}$ and step size α equal to $\frac{1}{2}$ (○), $\frac{1}{4}$ (×), $\frac{1}{8}$ (+), and $\frac{1}{16}$ (*). Initial separation $s=10^{-12}$. Realizations 1024.

In Fig. 1(a) we plot the RMS pair dispersion versus time for the four different time-step strategies, while in Fig. 1(b) we plot the logarithmic derivative of RMS pair dispersion $[\sigma(t)]$. Here and elsewhere in this paper, for all graphs of RMS pair dispersion versus time, we have rescaled space and time, respectively, via the initial separation distance, s, and the initial eddy turnover time $\tau_e(s)$ in order to display the number of spatial decades of pair separation achieved in each simulation.

In the time step validation study depicted in Fig. 1, we have the relatively modest range of nearly four decades of pair separation for each of the four parameter values. The graph in Fig. 1(a) visually displays convergence as α decreases from $\alpha=\frac{1}{2}$ to $\alpha=\frac{1}{16}$, while Fig. 1(b) indicates that all four cases have confirmed Richardson's t^3 scaling law over almost two spatial decades of RMS pair dispersion.

Finally, we report an even more stringent convergence test for the time-step strategy as the parameter α increases. We took the RMS dispersion $\sigma(t)$ and divided by $t^{1.5}$ and

computed $\sigma(t)/t^{1.5}$ at the last time, $t=10^3$ depicted on the graphs in Fig. 1. We denote this number by $\theta(\alpha)$. We have the following results:

$$\alpha=\tfrac{1}{2}, \quad \theta(\alpha)=0.22,$$

$$\alpha=\tfrac{1}{4}, \quad \theta(\alpha)=0.20,$$

$$\alpha=\tfrac{1}{8}, \quad \theta(\alpha)=0.18,$$

$$\alpha=\tfrac{1}{16}, \quad \theta(\alpha)=0.17,$$

which demonstrate the convergence of this statistical quantity as α decreases. Clearly, the value of $\alpha=\frac{1}{8}$ is sufficient for reasonable accuracy in this constant, and we utilize this value in the variable time-step strategy for all simulations reported in Secs. III and IV.

III. PAIR SEPARATION STATISTICS OVER MANY DECADES WITH KOLMOGOROFF SCALING

Here we present the results of Monte Carlo simulations for pair separation statistics that utilize the algorithm described in Sec. II with a Kolmogoroff random velocity field, $H=\frac{1}{3}$, and variable time step strategy with $\alpha=\frac{1}{8}$. We utilized an initial separation distance $s=10^{-14}$ and computed the averages over 1024 realizations.

In Fig. 2, we graph the pair dispersion statistics over many decades of pair separation. The graph of RMS dispersion in Fig. 2(a) indicates that power law behavior of pair dispersion occurs after about $t=10^2$ (100 initial eddy turnover times) and persists for eight decades of pair separation. The graph of the logarithmic derivative of pair dispersion versus time in Fig. 2(b) oscillates mildly with a mean value 3, which provides a stringent confirmation of Richardson's t^3 law. The logarithmic derivative shows the accuracy of the t^3 power law for every point in time $t>10^2$, whereas the least squares fit of RMS dispersion, which we discuss below, shows a crude average power for $t>10^2$.

Finally, Fig. 2(c) measures the Richardson constant and its variation over the scaling regime. In Fig. 2(c) we graph the pair dispersion divided by $t^3, \sigma^2(t)/t^3$, from our Monte Carlo simulation. Remarkably, as the reader can see by comparing Figs. 2(a) and 2(c), the Richardson constant settles down over more than 7.5 decades of pair separation, with the value 0.031 ± 0.004.

Next, we discuss the importance of rare events in the pair separation statistics. Given the mean flow $\bar{w}$, we consider the parallel and perpendicular components of the pair separation in a given realization defined, respectively, by

$$\mathbf{w}\cdot(\mathbf{X}_1^t-\mathbf{X}_2^t) \quad \text{and} \quad \mathbf{w}^{\perp}\cdot(\mathbf{X}_1^t-\mathbf{X}_2^t). \tag{16}$$

For any zero mean random variable u, the skewness, $S(u)$, and the flatness, $F(u)$ are the normalized constants, given by

$$S(u)=\frac{\langle u^3\rangle}{\langle u^2\rangle^{3/2}}, \quad F(u)=\frac{\langle u^4\rangle}{\langle u^2\rangle^2}.$$

For a Gaussian random variable, we have $S(u)=0$ and $F(u)=3$.

Next, we evaluate the skewness and the flatness of the parallel and perpendicular components of pair separation from the Monte Carlo simulation as time varies. The skew-

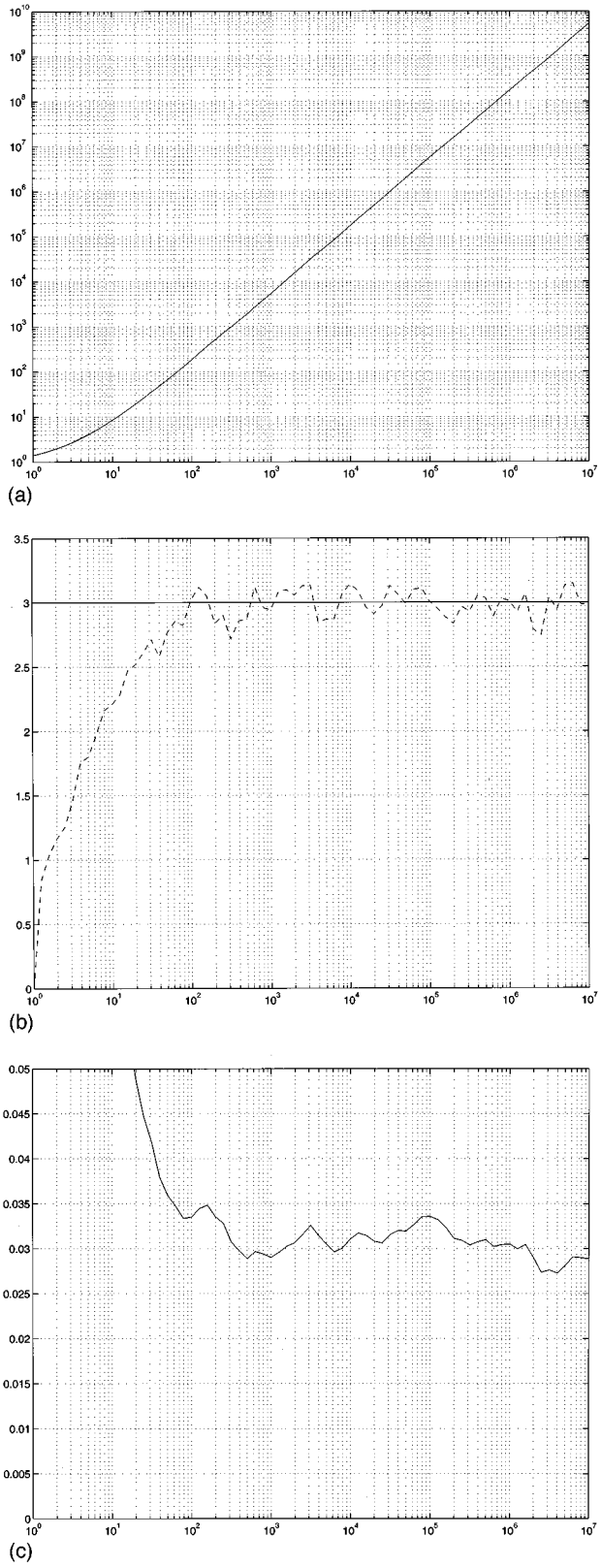

FIG. 2. Plots of (a) RMS dispersion versus time and (b) the logarithmic derivative of mean squared dispersion versus time. In (b) the solid line indicates $\gamma=3$ predicted by formula (6). (c) is a plot of the mean squared dispersion divided by t^3 versus time, indicating a Richardson constant of 0.031 ± 0.004 (for $t>10^2$) over nearly eight decades of pair separation. The y axis in (c) has range 0.00–0.05. Hurst exponent $H=\frac{1}{3}$. Initial separation $s=10^{-14}$. Realizations 1024.

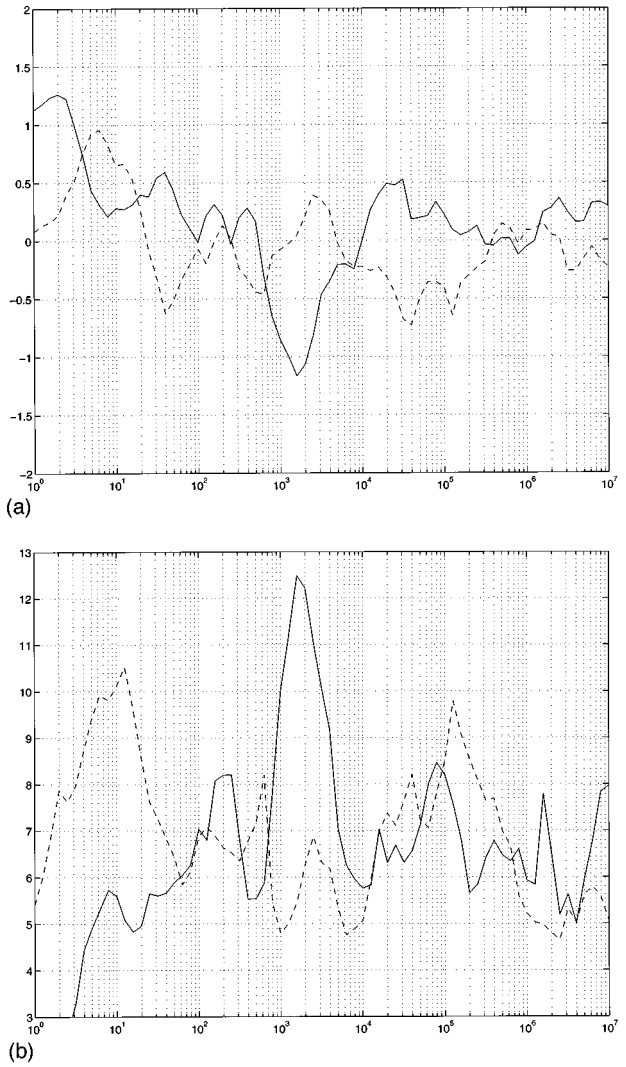

FIG. 3. Plots of (a) skewness of particle separation versus time and (b) flatness of particle separation versus time with $H=\frac{1}{3}$. Parallel component graphed with a solid line. Perpendicular component with a broken line. Initial separation $s=10^{-14}$. Realizations 1024.

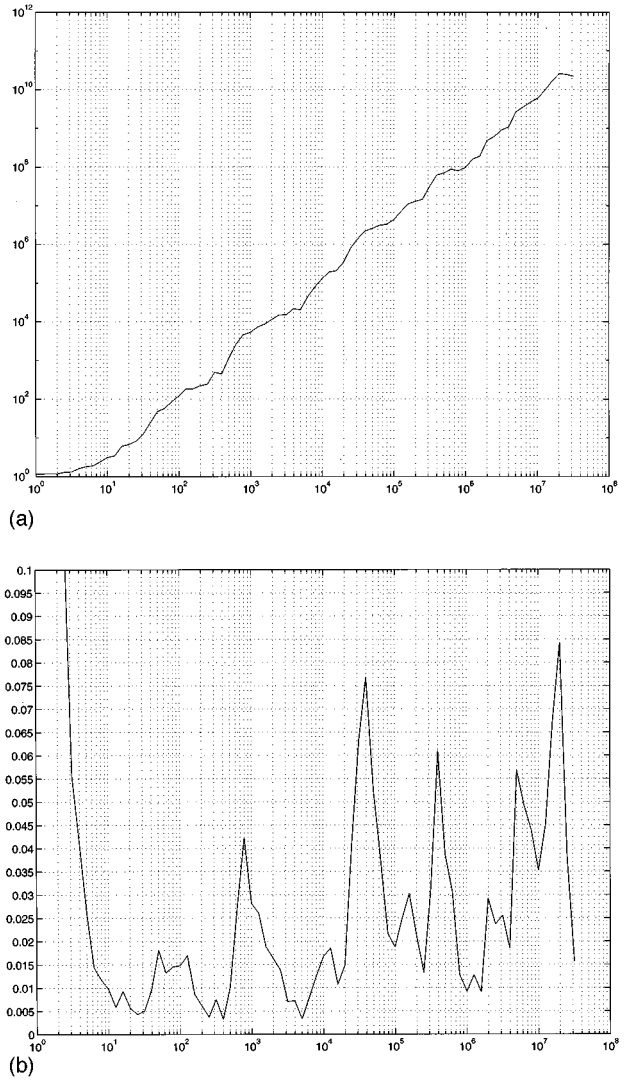

FIG. 4. Plots of (a) RMS dispersion versus time; (b) mean squared dispersion divided by t^3 versus time with Hurst exponent $H=\frac{1}{3}$ and two realizations. Note that the scale here for the y axis runs from 0.00 to 0.10 and there is wide scatter compared with the plot in Fig. 2(c), where all the variation is confined between 0.025 and 0.035.

ness for these two components is graphed in Fig. 3(a), while the flatness for these two components is graphed in Fig. 3(b). In these graphs, the parallel component of the separation is indicated by a solid line while the perpendicular component is denoted by a dotted line. After time, $t=10^2$, which indicates the onset of t^3 scaling behavior for pair dispersion, the two components of skewness are roughly symmetric about zero and almost always lie between -0.5 and $+0.5$. This provides a rough indication that the pair separation statistics are likely to have a symmetric distribution. As depicted in Fig. 3(b), the two components of flatness are almost always between the values of 5 and 8, after time $t=10^2$. Since the flatness of any Gaussian random variable is 3, this fact indicates that the probability density for pair separation has a much broader tail than a Gaussian throughout the entire t^3 scaling regime. The confidence levels in the fourth moment statistics preclude an accurate reporting of higher-order moments, as well as a full probability density function.

Another manifestation of the importance of rare events in the pair separation statistics is the variance in computed behavior of pair dispersion averaged over only a small number of realizations. In Fig. 4(a) we graph the RMS dispersion averaged over only two pairs of particles initially separated by 10^{-14}. Clearly, we see the expected nonmonotone behavior of pair separation for each individual realization. Nevertheless, the least squares fit of the RMS dispersion with two pairs of particles beyond time $t=10^2$ yields an exponent of 1.505 over eight decades of separation, confirming the Richardson t^3 law in a very crude time-averaged fashion. However, a graph of the logarithmic derivative of pair dispersion for two particle pairs (not depicted here) shows tremendous scatter with a minimum value of -0.90 and a maximum value of 8.07, in contrast to the data in Fig. 2(b), which indicates small scatter with averaging over 1024 realizations. The pair dispersion divided by t^3 for two particle pairs is graphed in Fig. 4(b). After the time $t=10^2$, the Richardson constant computed from two pairs of particles has the aver-

age value of 0.026 over eight decades of pair separation, with a wide scatter ranging from a minimum of 0.003 to a maximum value of 0.084 over eight decades of separation. Nevertheless, the averaged value for the constant with only two realizations, 0.026, is close to the value 0.031 ± 0.004 obtained over the entire eight decade range, with 1024 realizations and depicted earlier in Fig. 2(c).

IV. THE EFFECT OF ANISOTROPY IN THE VELOCITY SPECTRUM ON PAIR DISPERSION

As we mentioned briefly in Sec. II, one of the main computational devices in the Monte Carlo algorithm from Ref. 12 is to approximate an isotropic incompressible Gaussian random field over a large finite number of plane wave directions involving simple shear layers.[15] If, instead, only a small number of independent shear layer directions, for example only two directions, are utilized, then the corresponding random field is anisotropic with ordered behavior at each scale but with, nevertheless, a similar energy spectrum, as in the isotropic case. Here we use this technical device, together with the same adaptive time-stepping procedure described in Sec. II to develop Monte Carlo simulations for pair dispersion over many decades in random anisotropic fields, in contrast to the isotropic situation discussed earlier.

First, we briefly summarize the random plane wave decomposition from Refs. 12 and 15. We want to build systematic approximations involving random plane waves to an isotropic incompressible Gaussian random field with the velocity structure function in (2). To achieve this we let $\{v_j | j=0,1,2,...\}$ be a sequence of independent and identically distributed, one-dimensional, scalar Gaussian fields, satisfying

$$\begin{aligned} &\langle v_j \rangle = 0, \\ &\langle |v_j(x+x') - v_j(x')|^2 \rangle = |x|^{2\mathrm{H}}. \end{aligned} \tag{17}$$

For each M, we build the random plane wave approximations,[12,15]

$$\mathbf{v}_M(\mathbf{x}) = \left(\frac{\pi}{MC(H)} \right)^{1/2} \sum_{j=0}^{M-1} v_j \left[\left(\mathbf{x} \cdot \mathbf{u} \left(\frac{\pi j}{M} \right) \right) \right] \times \mathbf{u} \left[\pi \left(\frac{j}{M} + \frac{1}{2} \right) \right], \tag{18}$$

where $\mathbf{u}(\theta) = \cos(\theta)\mathbf{e}_1 + \sin(\theta)\mathbf{e}_2$. If we select the constant $C(H)$ in (18) so that

$$C(H) = \frac{\Gamma(\frac{1}{2})\Gamma(H+\frac{1}{2})}{2(H+1)\Gamma(H+1)},$$

then as $M \to \infty$ the random plane wave field from (18) converges to the isotropic incompressible Gaussian random field satisfying (10) and (11) with the constant $\tilde{C}_{\mathrm{H}} = 1$, i.e. satisfying the nondimensionalization of (13) in this paper. In fact, we use this formula with $M=16$ to yield an approximation that is very nearly isotropic[12] in the algorithm described in Sec. II. These 16 plane waves divide the unit circle into 32 equal arcs or ''shearing directions,'' as claimed in the Introduction and in Ref. 10.

If we use the formula in (18) with $M=2$ and $H=\frac{1}{3}$, we have random arrays of coherent eddies oriented along the coordinate axes with an anisotropic Kolmogoroff spectrum. The velocity structure function for the field in (18) with $M=2$ scales like $|x|^{2/3}$ but depends on the angle ϕ with the x_1 axis, i.e. the constant C_{H} from (10) and (11) is a function of the angle ϕ. A graph of the function $C_{\mathrm{H}}(\theta)$ is depicted in Fig. 5(a); we remind the reader for comparison that with the normalizations from (10), (11), and (13) in this paper, the isotropic value of C_{H} is 2.67. The graph of the anisotropic longitudinal structure function for $M=2$ in Fig. 5(b) shows a similar dependence on angle with the significant additional fact that this function vanishes identically at $\phi=0°$ and $\phi=90°$.

How much does the Richardson t^3 law for a pair dispersion change in such a structured random field, with the Kolmogoroff spectrum under Taylor's hypothesis? We varied the angle between the mean flow $\bar{w}$ and the x_1-coordinate axis systematically and applied the Monte Carlo algorithm from Sec. II with $M=2$ and 1024 realizations to study this issue. In these simulations, we utilized an initial separation distance $s=10^{-12}$ and ran our code for somewhat shorter times than described earlier in Sec. III, so that scaling behavior in pair dispersion was obtained over at least three decades of pair separation. The pair dispersion scaling exponent, γ, defined by $\sigma^2(t) = \beta t^{\gamma}$ for $t \gg 1$, is graphed in Fig. 5(c) as a function of the angle, ϕ, of the mean flow, $\bar{w}$, with the x_1-coordinate axis. In all such cases, we find that the pair dispersion over this three decade scaling range proceeds at a slower rate of spreading on the average than the t^3 law obtained earlier in Fig. 2 for an isotropic velocity field. For a sampling of angles between the mean flow and the x_1-coordinate axis, the exponent γ varies between 2.98 and 2.92. Furthermore, from Fig. 5(c) we observe that the pair dispersion exponent, γ, drops to its minimum value of 2.92 when the mean flow and the coordinate axis make the smallest computed angle of 6°. This is not difficult to understand intuitively because the longitudinal component of the structure function vanishes at the zero angle in this anisotropic setting [see Fig. 5(b)], and the large-scale sweep tends to localize more particle pairs in the direction along the x_1 axis where, from Eq. (9), the pair separation necessarily proceeds more slowly.

There are intuitive reasons to expect reduced pair dispersion in the situation described here. The fluid flow with $M=2$ is highly structured, and pair dispersion, in general, is arrested by pairs of particles remaining roughly aligned in directions of pair separation, where the longitudinal structure function vanishes. To elucidate these differences, in Fig. 6 we graph for a typical realization both the flow field in the nearly isotropic case utilized earlier in Sec. III and the flow field in the structured case with $M=2$, which we have just described.

Finally, we end this section with an important remark. We have also studied pair dispersion in the anisotropic situation with $M=4$ in Eq. (18). This value of M is already large enough for the random field to look completely disordered, and our computational results in this case (not reported here) essentially confirm Richardson's t^3 law with nearly the same accuracy as for the isotropic results presented earlier in this

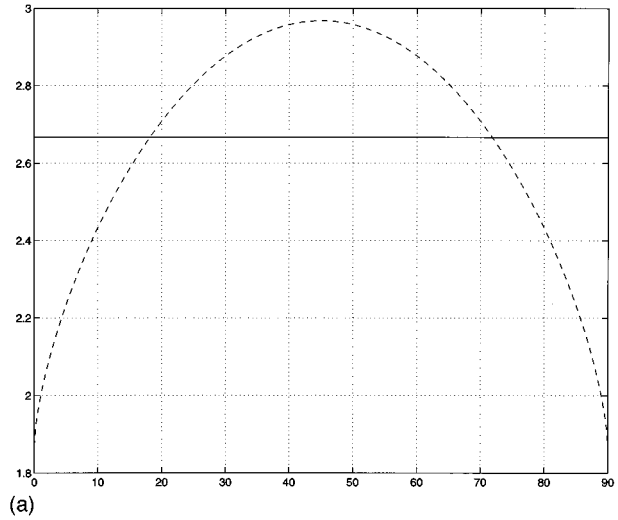

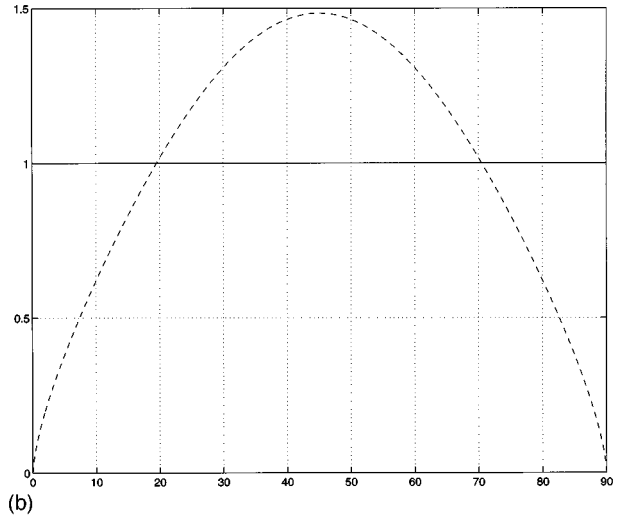

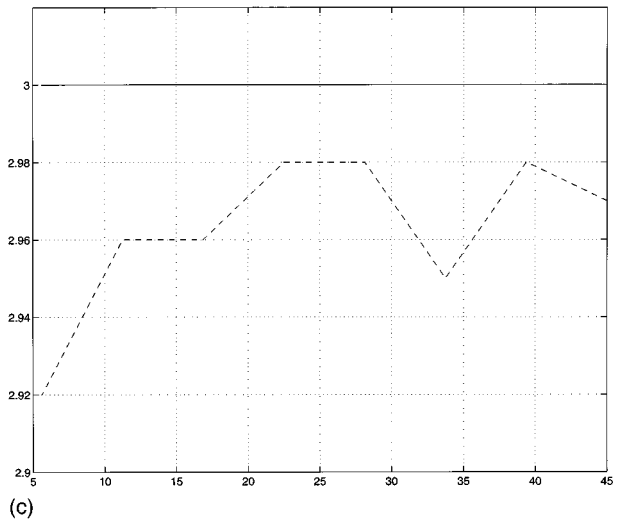

FIG. 5. Plots of (a) the structure constant $C_{\mathrm{H}}(\phi)$ and (b) the longitudinal structure constant $\tilde{C}_{\mathrm{H}}(\phi)$. Note that $\tilde{C}_{\mathrm{H}}(\phi)$ vanishes at $\phi=0$; (c) the simulated exponent γ vs ϕ for an isotropic field with two shearing directions and Hurst exponent $H=\frac{1}{3}$. The value of γ drops to 2.92 as the direction of sweep nearly becomes parallel with a coordinate axis where $\tilde{C}_{\mathrm{H}}(\phi)$ vanishes.

section. We have argued earlier that there are special directions where pair dispersion is arrested for the situation with

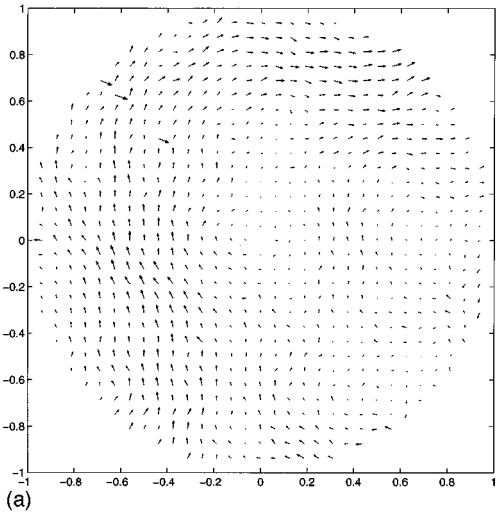

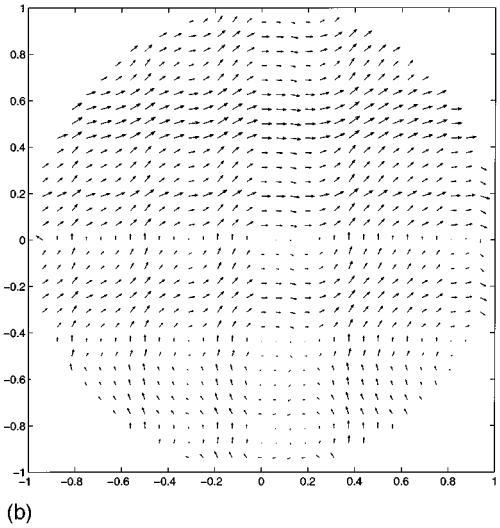

FIG. 6. Plots of a typical realization of (a) an isotropic velocity field and (b) an anisotropic field with two shearing directions and Hurst exponent $H=\frac{1}{3}$.

$M=2$, because the general formula in (9) applies and the longitudinal velocity structure function vanishes in these directions [see Fig. 5(b)]. On the other hand, a plot similar to the one in Fig. 5(b) for the case with $M=4$ confirms that the longitudinal structure function never vanishes at any angle in this case, and this is a significant reason for the validity of the t^3 law in this situation. Thus, the case of a velocity field with random plane waves and $M=2$ is exceptional in many respects; nevertheless, our numerical results do seem to confirm the possibility that there are some exceptional anisotropic ordered random flows with the Kolmogoroff spectrum, where, under Taylor's hypothesis alone, Richardson's t^3 law may not be satisfied.

V. PAIR DISPERSION UNDER TAYLOR'S HYPOTHESIS WITH VARYING VELOCITY SPECTRA

Here we report the results of Monte Carlo simulations with the numerical algorithm described in Sec. II to compute pair dispersion in an anisotropic velocity field with a varying Hurst exponent H, from (2), defining its spectrum under the

TABLE I. The Richardson exponent γ [see Eq. (6)] as a function of the Hurst exponent H. In all cases, initial separations $s=10^{-12}$ and 1024 realizations used. Average, minimum, and maximum calculated from logarithmic derivative of mean squared dispersion for time greater than 100 eddy turnover times, $t>10^2$.

Hurst exponent	Richardson exponent (γ)				Separation (decades)
	Predicted	Average	Minimum	Maximum	
0.2	2.50	2.48	2.27	2.75	6.2
0.3	2.86	2.83	2.64	2.99	5.7
0.4	3.33	3.30	3.20	3.46	4.2

assumptions of Taylor's hypothesis. We are especially interested in checking the validity of the theoretically predicted scaling law[6,9] for pair dispersion from (7), which generalized Richardson's law to other velocity fields with a general Hurst exponent, H.

For the results of the numerical simulations reported here, we began with an initial separation distance $s=10^{-12}$ with the nondimensionalization from (13), and in each case we utilized the Monte Carlo method from Sec. II with 1024 realizations.

We varied the Hurst exponent through the three values $H=0.2$, 0.3, and 0.4. In all three cases, the graphs for pair dispersion qualitatively resembled those described earlier in detail in Fig. 2 for the case of the Kolmogoroff spectrum with $H=\frac{1}{3}$; after an initial period of order 10^2 eddy turnover times, the pair dispersion settled into a power law scaling regime,

$$\sigma^2(t)=\beta t^{\gamma}, \quad t\gg 1, \tag{19}$$

for many decades of pair separation.

In Table I we compare the theoretically predicted scaling exponent $2/(1-H)$ from (7) with the average exponent γ computed over many decades of pair separation for the cases with $H=0.2$, 0.3, and 0.4. We also present the minimum and maximum of the local exponent determined from the logarithmic derivative in the scaling regime, as depicted earlier in Fig. 2(b), for $H=\frac{1}{3}$ and the number of decades of pair separation where this scaling behavior was achieved in each case. In all three cases, the computed exponent, γ, agreed with the theoretical exponent $2/(1-H)$ within the small error 0.03. Thus, the theoretical predictions of (7) for pair dispersion are confirmed by our Monte Carlo simulations within the numerical precision.

We observe from Table I that the number of decades of pair separation where scaling has been achieved decreases as the value of H increases. For a given initial separation distance, the reasons are computational; we only have computer resources to generate all the (over 2^{50}!!) Gaussian random variables by the method of Ref. 12 for the velocity field in the unit circle. At the larger values of the Hurst exponent, particles escape from the unit circle more rapidly, and the computation must be terminated before this happens. We achieved more decades of scaling behavior for pair separation for the Kolmogoroff spectrum in Sec. III by picking an even smaller initial pair separation, $s=10^{-14}$.

VI. CONCLUDING DISCUSSION

A. The Richardson constant

The main result presented in this paper is confirmation of Richardson's t^3 law for pair dispersion over a range of pair separation spanning eight decades. In fact, the Richardson constant has the value 0.031 ± 0.004 over nearly eight decades of pair separation for an isotropic Kolmogoroff velocity field under Taylor's hypothesis, provided that the longitudinal component of the velocity structure tensor is normalized to unity. These results were achieved with a new Monte Carlo method developed recently by the authors[11,12,16] with the capability of generating many decades of scaling behavior through a Gaussian random velocity field with the Kolmogoroff spectrum. Since the value of Richardson's t^3 law has been the object of extensive experimental,[2,3,17] theoretical,[4–7] and numerical[8,10] investigation in various contexts, we compare the results obtained here with those developed elsewhere.

To do this, we use more conventional notation from turbulence theory, where the longitudinal component of the velocity structure tensor with Kolmogoroff's law is given by

$$\left\langle \left([\mathbf{v}(\mathbf{x}+\mathbf{x}')-\mathbf{v}(\mathbf{x}')]\cdot \frac{\mathbf{x}}{|\mathbf{x}|} \right)^2 \right\rangle = C_L \bar{\epsilon}^{2/3} |x|^{2/3}, \tag{20}$$

and C_L is a universal constant from turbulence theory related to the Kolmogoroff constant. The Richardson law for pair dispersion assumes the form

$$\sigma^2(t)=G_{\Delta}\bar{\epsilon}t^3, \tag{21}$$

where G_{Δ} is the Richardson constant. The experimental measurements[18] give a value of $C_L=2.0\pm0.1$, and a value of $C_L\simeq 2$ is obtained in three dimensions with a choice of the spectral Kolmogoroff constant $C_K=1.5$

Thus, with (20) and (21) we use the value $C_L=2$ so that the Monte Carlo simulations developed here in two space dimensions with an isotropic Kolmogoroff spectrum under Taylor's hypothesis predict a Richardson constant,

$$G_{\Delta}=0.062\pm0.008, \tag{22}$$

valid over nearly eight decades of pair separation. Remarkably, the value (22) agrees with the one obtained by Tatarski, $G_{\Delta}=0.06$, in his experiments; Ozimodov[17] has also argued from his experimental data that the appropriate range for G_{Δ} is $O(.1)$. Sabelfeld studied pair dispersion under Taylor's hypothesis over crude separation distances (by the standards of this paper) involving only one decade of pair separation and obtained the value, $G_{\Delta}=0.24\pm0.03$. Fung *et al.*,[10] in an interesting paper, did not study the behavior of Richardson's law under Taylor's hypothesis, but, instead, built synthetic turbulent velocity fields with spatiotemporal Kolmogoroff statistics where the scaling in (20) was satisfied for less than one decade (in contrast to the 15 decades in the methods utilized here); nevertheless, the Richardson t^3 law was observed for a couple of decades of pair separation with a constant $G_{\Delta}=0.1$, where these authors assumed $C_K=1.5$, so that $C_L\simeq 2$. All of the work just mentioned points to a small value of the Richardson constant, G_{Δ}, and our direct simulations spanning many decades of pair separation confirm a small

value for $G_\Delta = 0.062 \pm 0.008$ under the assumptions of Taylor's hypothesis over an extremely long scaling range for pair dispersion.

On the other hand, turbulence closure theories[4–7] produce values of G_Δ that are nearly two orders of magnitude larger. With LHDI, Kraichnan[4] predicted $G_\Delta = 2.42$, with modified LHDI, Lundgren[5] predicted $G_\Delta = 3.00$, an EDQN procedure[6] leads to $G_\Delta = 3.50$, and a random flight model has $G_\Delta = 2.00$. What are the reasons for the wide discrepancies between these closure theories and the results mentioned in the previous paragraph regarding the predicted value of G_Δ?

Perhaps, these turbulence theories are applied in a regime of spatiotemporal spectra for the velocity field, which is very far from the circumstances of Taylor's hypothesis. There is unambiguous mathematical evidence[14,15] that the nature of the spatiotemporal velocity spectrum can have a substantial influence on pair dispersion. For example, for an isotropic incompressible velocity field with the spatial spectrum in (2) for any Hurst exponent, H, but with *short-range temporal correlation independent of spatial wave number*, rigorous theory[15] establishes that the pair dispersion scales like

$$\sigma^2(t) = \beta t^{1/(1-H)}, \quad t \gg 1, \tag{23}$$

and this exponent is *one-half* the one from (7), which we have just confirmed under Taylor's hypothesis in Sec. V of this paper. On the other hand, the interesting numerical study in Ref. 9 suggests that there are even velocity fields without a sufficient scaling regime where Richardson's t^3 law remains valid; we consider the interesting work of Fung *et al.*[10] to be essentially another example of this phenomenon.

B. Future directions

With the above discussion, a very interesting research direction is to develop reliable Monte Carlo methods to simulate pair separation statistics with velocity fields having both a large-scale sweep and a spatiotemporal spectrum ranging over many scales.[14] With such a method, all of the competing effects of velocity structure on pair dispersion could be studied in a controlled fashion. Furthermore, the interesting effects of anisotropy in random structured velocity fields in reducing pair dispersion, as studied under Taylor's hypothesis in Sec. IV, warrant further investigation in this broader context. Such a numerical method has been developed by the authors very recently by modifying the procedure utilized here, and the results of numerical experiments on all of these issues will be reported elsewhere in the near future.

ACKNOWLEDGMENTS

The work of Frank Elliott and Andrew Majda was supported by grants from the National Science Foundation, the Office of Naval Research, and the Army Research Office. Most of the calculations in this paper were performed on the Cray T3D at the Pittsburgh Supercomputing Center of the National Science Foundation.

[1] L. Richardson, "Atmospheric diffusion shown on a distance-neighbor graph," Proc. R. Soc. London Ser. A **110**, 709 (1926).
[2] V. Tatarski, "Radiophysical methods of investigating atmospheric turbulence," Izv. Vyssh. Ucheb. Zaved. 3 Radiofiz. **4**, 551 (1960).
[3] A. Monin and A. Yaglom, *Statistical Fluid Mechanics* (MIT Press, Cambridge, 1975), Vol. 2.
[4] R. Kraichnan, "Dispersion of particle pairs in homogeneous turbulence," Phys. Fluids **9**, 1728 (1966).
[5] R. Lundgren, "Turbulent pairs dispersion and scalar diffusion," J. Fluid Mech. **111**, 25 (1981).
[6] M. Larcheveque and M. Lesieur, "The application of eddy-damped Markovian closures to the problem of dispersion of particle pairs," J. Mech **20**, 113 (1981).
[7] D. Thomson, "A stochastic model for the motion of particle pairs in isotropic high Reynolds number turbulence, and its application to the problem of concentration variance," J. Fluid Mech. **210**, 113 (1990).
[8] K. Sabelfeld, *Monte Carlo Methods* (Springer-Verlag, New York, 1991), Chap. 5.3, pp. 228–245.
[9] N. Zovari and A. Babiano, "Derivation of the relative dispersion law in the inverse energy cascade of two-dimensional turbulence," Phys. D **76**, 318 (1994).
[10] J. Fung, J. Hunt, N. Malick, and R. Perkins, "Kinematic simulation of homogeneous turbulence by unsteady random Fourier modes," J. Fluid Mech. **236**, 281 (1992).
[11] F. Elliott and A. Majda, "A wavelet Monte Carlo method for turbulent diffusion with many spatial scales," J. Comput. Phys. **113**, 82 (1994).
[12] F. Elliott and A. Majda, "A new algorithm with plane waves and wavelets for random turbulent velocity fields with many spatial scales," J. Comput. Phys. **117**, 146 (1995).
[13] D. Horntrop and A. Majda, "Subtle statistical behavior in simple models for random advection diffusion," J. Math. Sci. Univ. Tokyo **1**, 23 (1994).
[14] M. Avellaneda and A. Majda, "Mathematical models with exact renormalization for turbulent transport, II: Non-Gaussian statistics, fractal interfaces, and the sweeping effect," Commun. Math. Phys. **146**, 139 (1992).
[15] A. Majda, "Random shearing direction models for isotropic turbulent diffusion," J. Stat. Phys. **75**, 1153 (1994).
[16] F. Elliott, A. Majda, D. Horntrop, and R. McLaughlin, "Hierarchical Monte Carlo methods for fractal random fields," J. Stat. Phys. **81**, 717 (1995).
[17] R. Ozmidov, "On the rate of dissipation of turbulent energy in sea currents and in the dimensionless constant in the '4/3 power law'," Izv. Akad Nauk SSSR. Ser. Geotiz. 821 (1960).
[18] A. Townsend, *The Structure of Turbulent Shear Flow* (Cambridge University Press, Cambridge, 1976).
[19] D. Horntrop (private communication).